# The crystal structure of $Mg_8(Mg_2Al_2)Al_8Si_{12}(O,OH)_{56}$ pumpellyite and its relevance in ultramafic systems at high pressure

## G. ARTIOLI,* P. FUMAGALLI, AND S. POLI

Dipartimento di Scienze della Terra, Università di Milano, Via Botticelli 23, I-20133 Milano, Italy

## ABSTRACT

Multianvil experiments in the model system $MgO\text{-}Al_2O_3\text{-}SiO_2\text{-}H_2O$ at 680 °C and 5.2-6.0 GPa yield a variety of Mg,Al-rich mineral assemblages containing pumpellyite-type phases. Run products include the assemblages pumpellyite-coesite, pumpellyite-forsterite-orthoenstatite and pumpellyite-10 Å phase. The pumpellyite-coesite sample contains pumpellyite with nominal composition $Mg_8(Mg_2Al_2)Al_8Si_{12}(O,OH)_{56}$ and about 6 wt% coesite. Powder diffraction data obtained using synchrotron radiation, a parallel-beam Debye geometry, a capillary sample mount, and an Image Plate were refined by Rietveld structure analysis. The structure was modeled in space group $P2_1/m$ [cell $a = 8.5759(4)$, $b = 5.7295(2)$, $c = 18.5376(9)$ Å, $\beta = 97.691(3)°$, $V = 902.66(9)$ Å$^3$] and shows extensive stacking disorder along the [001] direction, which can be described as layers of X-octahedra shifted by (1/2,0,0) vectors. The shifted layers locally show a sursassite-type arrangement. No disorder was detected in the Y-octahedra, which are fully occupied by Al ions, and in the W positions, commonly hosting sevenfold-coordinated Ca atoms in naturally occurring pumpellyite minerals, whereas in the synthetic Mg-rich pumpellyite they are fully occupied by Mg atoms in a distorted sixfold-coordination. The structure can then be described as a pumpellyite-type structure having a certain amount of sursassite domains. Alternative structure models involving: (1) possible presence of ardennite-domains; (2) a sursassite-type structure with pumpellyite domains; (3) cell doubling along $c$ due to long range ordering of the layers containing the X octahedra; or (4) a statistically disordered structure in the centered $A2/m$ parent space group and in other $t$ subgroups, were all tested and discarded on the basis of the full-profile Rietveld refinements of powder diffraction data. The selected model indicates that the polytypic behaviour observed in pumpellyite and related structures (sursassite, and possibly ardennite) is also possible in the high pressure members of the group. The volume of the reaction, $MgSiO_3$(enstatite) + 2 $Mg_2SiO_4$(forsterite) + $Mg_8(Mg_2Al_2)Al_8Si_{12}O_{42}OH_{14}$ (pumpellyite) $\leftrightarrow$ 5 $Mg_3Al_2Si_3O_{12}$(pyrope) + 7 $H_2O$ re-evaluated using the new crystallographic data, gave a negative $dP/dT$ slope. The assemblage chlorite-enstatite-pyrope acts as compositional barrier for the occurrence of pumpellyite in most ultramafic compositions for $H_2O$-undersaturated conditions. In more complex Fe,Ca-containing systems, the preferential partitioning of Fe,Ca in pumpellyite compared to garnet enhances its potential petrological importance in ultramafic subducting slabs.

## INTRODUCTION

Pumpellyite is a mixed group silicate containing isolated [$SiO_4$] tetrahedra and disilicate [$Si_2O_6(OH)$] groups. The general formula is commonly indicated as $W_8X_4Y_8Z_{12}O_{56-n}(OH)_n$, where W are sevenfold-coordinated sites commonly occupied by Ca, X and Y are two crystallographically independent octahedral sites occupied by divalent and trivalent cations, and Z indicates tetrahedral sites invariably occupied by Si (Passaglia and Gottardi 1973). Structure-analogues chemical variants of pumpellyite are the minerals julgoldite (Moore 1971; Allmann and Donnay 1973), shuiskite (Ivanov et al. 1981), okhotskite (Togari and Akasaka 1987), and V-pumpellyite (Pan and Fleet 1992). The mineral is to be named pumpellyite, julgoldite, shuiskite, or okhotskite where Al, Fe, Cr, or Mn, respectively,

is the prevailing cation in the Y-octahedral site. The structure and crystal chemistry of pumpellyite are closely related to a number of silicate minerals containing disilicate (sursassite, macfallite) or trisilicate groups (ardennite, orientite). All these minerals can be considered polytypes on the basis of order-disorder (OD)-theory, because their ideal OD-structures can be derived from two different kind of layer unit stacked in regular alternation (see Pasero and Reineke 1991, and references therein). Although the basic crystal structure of pumpellyite has been known for some time (Gottardi 1965; Galli and Alberti 1969; Yoshiasa and Matsumoto 1985), the crystal chemical role of mixed-valence elements in the structure has been investigated only recently (Artioli and Geiger 1994; Artioli et al. 1996; Akasaka et al. 1997).

Ca-free pumpellyite of nominal composition $Mg_5Al_5Si_6O_{21}(OH)_7$ was first synthesized by Schreyer et al. (1986, 1987, 1991) from a gel composition $5MgO:2.5Al_2O_3:6SiO_2$ in the presence of excess $H_2O$. The measured stoichi-

ometry of the mineral phase identifies it as an analogue of pumpellyite (Schiffmann and Liou 1980). Following the accepted nomenclature for pumpellyite-type minerals (Passaglia and Gottardi 1973), it should be labeled as pumpellyite-(Mg,Al), having Al as the prevailing cation in the Y position, and an ideally equal proportion of Mg and Al in the X position. However, no official nomenclature exists to indicate the prevailing cation in the W position, as all studied natural pumpellyite minerals contain Ca cations in this crystallographic site, with the only exception of a reported manganoan pumpellyite having extensive Ca substitution by Mn (Coombs et al. 1996).

Hence, we adopt the name proposed by Schreyer (MgMgAl-pumpellyite) because it is of widespread usage in the literature and clearly indicates the presence of Mg in the W sites, even though it does not strictly conform to the proposed nomenclature.

Stability relations in the simple system $MgO-Al_2O_3-SiO_2-H_2O$ (MASH) indicate that the MgMgAl-pumpellyite is stable above 3.4 GPa and at temperatures up to 820 °C. The low and high temperature stability limits are determined by the breakdown reaction to talc + Mg-carpholite + chlorite (400–600 °C, 3.7–4.5 GPa; Schreyer et al. 1991) and by the dehydration reaction to pyrope + kyanite + coesite + $H_2O$ respectively (730–770 °C, 5.0 GPa; Fockenberg 1998). The lower pressure limit is defined by the breakdown reaction to Mg-chloritoid + talc + Mg-carpholite. At pressures higher than 6.0 GPa MgMgAl-pumpellyite breaks down to Mg-chloritoid + talc + Mg-carpholite, to talc + kyanite + pyrope + $H_2O$ and to pyrope + kyanite + coesite + $H_2O$. In the simple MASH system and in ultramafic compositions, the MgMgAl-pumpellyite has relevance as a $H_2O$ reservoir which could transport and then release water at depth in the mantle by subduction zone processes. In particular its appearance is related to the reaction enstatite + chlorite ↔ forsterite + pumpellyite, whereas its upper thermal breakdown is related to the occurence of pyrope + $H_2O$ (Ulmer and Trommsdorff 1998). The topology of phase relations involving MgMgAl-pumpellyite, pyrope, chlorite, forsterite, enstatite, and $H_2O$ is still poorly understood. Furthermore, limited data indicate that MgMgAl-pumpellyite is also present in more complex systems including Ca and Fe at such pressures and temperatures (Domanik and Holloway 1996). Despite the widely recognized relevance of MgMgAl-pumpellyite as a water carrier in the mantle (Schreyer et al. 1991; Fockenberg 1998) its crystal structure is still unknown.

We report here its full chemical and structural analyses by electron probe microanalysis (EPMA) and synchrotron X-ray powder diffraction (SXRPD). Phase relationships are discussed in the light of present experimental constraints and crystal-chemical evidence.

## EXPERIMENTAL METHODS

### Synthesis techniques

Gels were used as starting materials. They were prepared following the method of Hamilton and Henderson (1968) using tetraethylorthosilicate (TEOS) as silica source, pure Mg and Al, nitric acid, and ammonium hydroxide. Bulk compositions fall close to the joins MgMgAl-pumpellyite-coesite, MgMgAl-pumpellyite-10 Å phase, and pyrope-enstatite (Fig. 1). Gels were run at 5.2 GPa and 680 °C for 116–311 hours

except for the bulk composition pyrope-enstatite which was also run at 6.0 GPa and 680 °C. Gold capsules (outer diameter 3.00 mm, length 3.5–4.5 mm) were welded after being loaded with 10–15 mg gel and 10 wt% distilled water.

Runs were carried out in a Walker-type multi anvil apparatus at the Dipartimento di Scienze della Terra, Milan. Tungsten carbide cubes of 32 mm edge length and 17 mm truncation edge length (TEL) were used. Pressure cells were made of pre-fabricated MgO octahedra (containing 5 wt% $Cr_2O_3$) with a 25 mm edge length (25 *M*). Assemblies were composed of stepped graphite heater, MgO spacers, and axial thermocouple (Pt-Pt90Rh10, S-type) insulated by a mullite ceramic and placed in direct contact with the capsule. Graphite discs on both the ends of the assembly provided electrical contact with the WC cubes (for details see Poli and Schmidt 1998).

Pressure calibration was performed both at room temperature, using the phase transitions BiI-II, BiIII-V (respectively at 2.6 and 7.7 GPa), and at 1000 °C, using the coesite-stishovite and $CaGeO_3$ garnet-perovskite transitions occurring respectively at 8.7 GPa (Zhang et al. 1996) and 7.7 GPa (Susaki et al. 1985). Pressure uncertainties, largely depending on the accuracy of the calibrant reaction, were assumed to be ±4%. Temperature was considered accurate to ±20 °C without taking into account the effect of pressure on the e.m.f. of the thermocouple.

Product mineral assemblages along with bulk compositions of starting materials are in Figure 1.

## Run results: phase identification

All runs were first characterized by conventional X-ray powder diffraction on a Philips PW1000 diffractometer and carefully inspected by backscattered and secondary electron SEM images. The MgMgAl-pumpellyite phase was detected in all
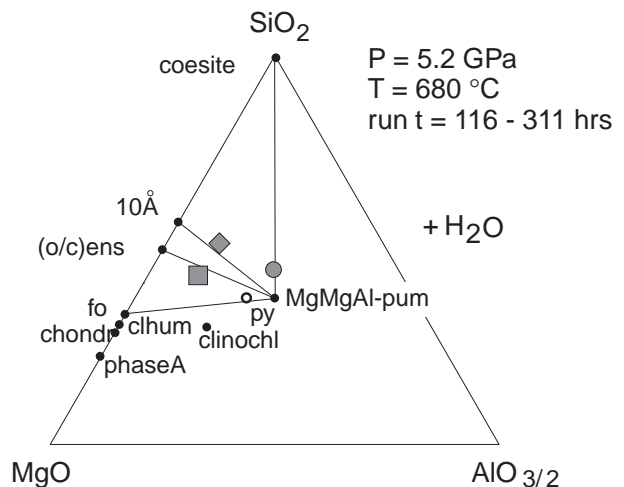


**FIGURE 1.** Bulk compositions and run products at 5.2 GPa and 680 °C. The sample lying near the enstatite-pyrope join was also run at 6.0 GPa and 680 °C obtaining the same products. (o/c)ens = ortho/clino-enstatite; fo = forsterite; clhum = clinohumite; clinochl = clinochlore; chondr = chondrodite; py = pyrope; MgMgAl-pum = MgMgAl-pumpellyite.

synthesis runs, always associated with coesite, with forsterite + orthoenstatite, or with coesite + 10 Å phase. The distinction between ortho- and clinoenstatite was difficult because their distinctive diffraction peaks overlap those of the other phases present, i.e., MgMgAl-pumpellyite and forsterite. However the results of the quantitative phase analyses carried out by Rietveld refinement method suggest the occurrence of orthoenstatite at 5.2 and 6.0 GPa and 680 °C, in agreement with Angel et al. (1992).

The 10 Å phase was recognized on the basis of its stoichiometry (MgO:SiO$_2$ = 3:4) and on the presence of the broad basal peak at $d$ = 10.10 Å in the powder diffraction pattern, in agreement with type I of Yamamoto and Akimoto (1977). The 10 Å phase invariably shows crystals (up to 100 μm) with platy hexagonal habit. The sample containing the least amount of additional phases was used for diffraction data collection.

An ARLK microprobe with six spectrometers was used for EPMA microanalyses. Beam conditions were set to 15 kV and 20 nA. Silicates were used as standards and data processed with a standard ZAF correction procedure. The mean composition of EPMA point analyses normalised on 16 cations indicates the following unit formula for MgMgAl-pumpellyite: Mg$_{5.056}$Al$_{4.994}$Si$_{5.950}$(O,OH)$_{28}$. The SEM image (Fig. 2) shows a well-developed prismatic crystal (>10 μm) of MgMgAl-pumpellyite.

### Synchrotron X-ray powder data collection

The powder diffraction data were collected at the D8 GILDA beamline (General Italian Line for Diffraction and Absorption) at the European Synchrotron Radiation Facility, Grenoble, France. The bending magnet beamline optics encompasses a double crystal Si monochromator, with the second crystal sagittally bent to focus the beam in the horizontal plane, and a vertically focusing Pt coated mirror (Pascarelli et al. 1996). A wavelength of 1.30365(2) Å was selected for the experiment
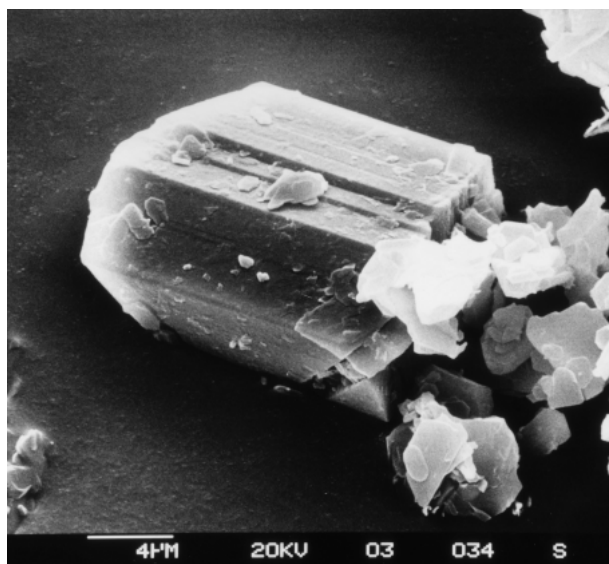


**FIGURE 2.** SEM image of a prismatic crystal of MgMgAl-pumpellyite synthesized at 5.2 GPa and 680 °C.

and calibrated against the reference silicon sample (NBS 640b, having $a$ = 5.430954 Å at 26 °C). The sample was hand ground, loaded into a 0.3 mm diameter Lindemann capillary, and attached to a standard goniometer head. The latter was mounted on the φ axis of a two-circle diffractometer and axially rotated during the data collection in Debye-Scherrer geometry. The whole diffraction rings were recorded on an Fuji Image Plate located at 17.3 cm from the sample, and perpendicular to the incident beam. The sample to detector and residual tilt angles were calibrated by analysis of the diffraction data obtained on standard Si and LaB$_6$ samples (NBS/NIST 640b and 660a, respectively) in the same experimental conditions. All calibrations and data processing were performed on the scanned digital images (Fuji BAS2000 Scanner) by the use of the Fit2d program package (Hammersley et al. 1996). The diffraction rings were radially integrated, and the intensities were corrected for flat plate geometrical distortion and polarization (polarization factor = 0.96). The intensity data were then interpolated to fixed angular steps, and converted into a conventional diffracted intensity vs. diffraction angle profile. The subsequent structure analysis was performed by full-profile Rietveld method using the GSAS software (Larson and Von Dreele 1998).

### RIETVELD STRUCTURE ANALYSIS

The starting structural model for pumpellyite was from Galli and Alberti (1969). Given the absence of Ca in the structure and the controlled stoichiometry, the W sites were initially considered to be occupied by Mg atoms alone, and the X and Y octahedral sites were modeled by full occupancy of Al cations. Although part of the latter sites ought to be occupied by Mg according to stoichiometry, the powder data are essentially insensitive to the presence of either one of the two iso-electronic species. In the subsequent structure analysis cation-oxygen bond length information was employed to unravel the site occupancies. The basic structure model was preliminarily kept fixed and employed to extract reasonable peak-profile parameters, a background-modeling curve, and initial unit-cell parameters. The same procedure was adopted when testing the structure model of sursassite following Mellini et al. (1984). The pumpellyite and sursassite structures can be considered different stacking arrangements of the same octahedral layer units (Mellini et al. 1984; Pasero and Reineke 1991). Again the Mn sites were considered as fully occupied by Mg atoms, and the X octahedral site was initially modeled by full Al occupancy. Preliminary Rietveld fits showed that: (1) coesite is present as an impurity phase, and therefore was inserted as a second phase in the refinement; and (2) small diffraction peaks are present neither accounted for by the pumpellyite ($A2/m$ space group) nor by the sursassite ($P2_1/m$ space group) structure models (Fig. 3). Bragg peaks not compatible with the sursassite structure were previously observed by Schreyer et al. (1991).

The two small peaks at $d$-spacing 8.01 and 7.26 Å (Fig. 3) are not present in the powder diffraction pattern of pumpellyite, but are present in the powder pattern of sursassite, and clearly indicate that a certain amount of sursassite domains exist in the investigated phase. The other two small peaks at $d$-spacing 3.21 and 3.18 Å are not present in either of the diffraction patterns and could in principle have several causes: (1) the presence of
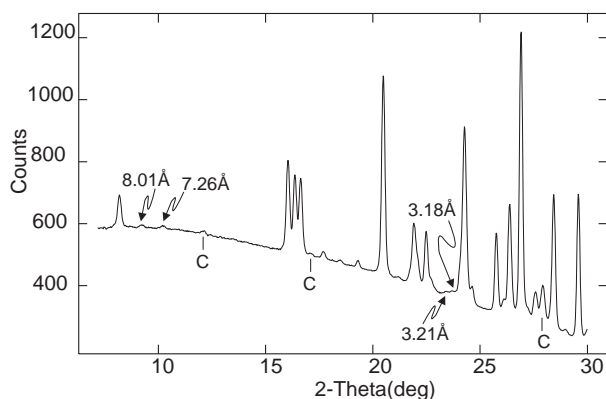
**FIGURE 3.** Selected portion of the experimental powder pattern of synthetic MgMgAl-pumpellyite collected by synchrotron radiation. "c" indicates the Bragg peaks attributed to coesite impurities. The two peaks at *d*-spacings 8.01 and 7.26 Å indicate a space group lower than the centered *A*2/*m* space group generally assumed for pumpellyite (see text for details).

additional ardennite domains within pumpellyite-sursassite polytypic structure; (2) the presence of additional Bragg peaks due to symmetry lowering within the pumpellyite structure; or (3) the presence of an additional Al-Mg-rich phase stable at high pressure. We emphasize that the modeling of the measured powder diffraction pattern using the pumpellyite or the sursassite structure models are both remarkably satisfactory in terms of the resulting crystal chemistry and of the profile agreement indices. However, all the above hypotheses were carefully tested to explain the presence of the observed additional diffraction peaks.

The presence of domains having an ordered ardennite-type stacking of the basic layer unit (i.e., octahedral layer units containing a mirror and forming $Si_3O_{10}$ groups: Ferraris et al. 1986, Pasero and Reineke 1991) was assessed by tentative multiphase Rietveld refinements. Insertion of Mg-ardennite as an additional phase clearly indicated the absence of extended domains of this phase within the experimental limits of detection.

Extensive search in the powder diffraction database (PDF-2) indicated that all candidate high pressure or low pressure phases showing the observed peaks at *d*-spacing 3.21 and 3.18 Å must in addition show major peaks at low diffraction angle. Since no such peak is observed, the hypothesis of an additional impurity phase besides coesite was discarded as well.

The possible symmetry lowering of the MgMgAl-pumpellyite structure was tested by performing extensive Rietveld modeling in the following "transationengleiche" primitive space groups (*t* subgroups): *P*2/*m*, *P*2$_1$/*m*, *P*2/*c*, *P*2$_1$/*c*. The refinement in the parent *A*2/*m* space group using the pumpellyite structure model, and the refinement in the *P*2$_1$/*m* space group using the sursassite structure model were also completed for comparison purposes (Table 1). The refinements using a cell doubled along *c* may be justified on the basis of long range order of the layer units forming the pumpellyite structure (Pasero and Reineke 1991), they were tested but were soon abandoned because none of these could properly account for the small additional Bragg peaks observed in the powder diffraction pattern, and furthermore the large num-

ber of parameters present in the models with doubled cell inevitably produced numerical correlation and divergence of the refinement.

The Rietveld refinements in the four primitive subgroups preserving the standard cell of pumpellyite were all rather successful in terms of convergence toward a stable minimum, and in terms of overall agreement factors. The results are shown in Table 1, together with the results of the refinement in the *A*2/*m* parent space group of pumpellyite and the results of the refinement of the sursassite model in the *P*2$_1$/*m* space group. Both structure models are shown in Figure 4 and following Pasero and Reineke (1991) they can be described in terms of stacking of octahedral layers having the 2 or 2$_1$ symmetry. The layer containing the X-octahedra is similar in the two structures and always has the 2$_1$ symmetry, whereas the layer containing the Y-octahedra has the 2 symmetry in pumpellyite (Fig. 4 top) and the 2$_1$ symmetry in sursassite (Fig. 4 middle). The different symmetry of the Y-layer is essentially determined by the relative shift of adjacent X-layers.

All subgroup refinements produced a reasonable fit, and a very similar general interpretation of the structure. All models imply that: (1) the Mg atoms located in the W sites (Ca sites in pumpellyite or Mn sites in sursassite) have a distorted octahedral coordination and are fully occupied. Although two of the Mg atoms could be considered to be almost sevenfold-coordinated on account of their distances to the next nearest oxygen atom (Mg2-O6 = 2.59 Å; Mg3-O15 = 2.43 Å), the other two Mg atoms are too far from the next nearest oxygen atom to be considered within bonding distance (Mg1-O4 = 3.03 Å; Mg4-O17 = 3.09 Å). (2) The octahedral Y sites are fully occupied by Al cations, on account of the mean cation-oxygen bond lengths (1.933 and 1.948 Å for Y-Al1 and Y-Al2 respectively: Table 2). (3) There is a substantial degree of disorder in the layer units containing the X-octahedra.

The X-layer disorder is confirmed by the fact that values substantially lower than 1.0 are obtained by refining the site occupancy factor of the X-octahedral cation site both in the sursassite and in the pumpellyite parent model. This observation is consistent with the observed polytipic behavior of the pumpellyite structure (Mellini et al. 1984; Pasero and Reineke 1991) and it might be related to the synthesis conditions. In principle it can expected that different synthesis conditions may produce any degree of stacking disorder between end-member pumpellyite and sursassite structures.

The observed disorder implies that some of the X-layers do not obey a rigorous long range order and are locally shifted by (1/2,0,0) vectors. The resulting structure could in theory be described equally well using three models: (1) a parent pumpellyite *A*2/*m* model containing sursassite-type domains; (2) a sursassite *P*2$_1$/*m* model containing pumpellyite-type domains; (3) a pumpellyite-type model having a lower space group symmetry and showing some disorder on the octahedral and tetrahedral layers within the X-layer.

Model 3 is here preferred because it is the only one that fully accounts for all the observed additional peaks in the powder diffraction pattern. On the basis of this defect-structure model, the search for a possible symmetry subgroup of *A*2/*m* is reduced to the analysis of possible symmetry correlation be-

**TABLE 1.** Results of the Rietveld refinement of the synchrotron powder diffraction of MgMgAl-pumpellyite in the parent *A 2/m* space group of pumpellyite and in four *t* subgroups

| Structure model space group | pumpellyite A2/m | pumpellyite P2/m | pumpellyite P2₁/m | pumpellyite P2/c | pumpellyite P2₁/c | sursassite P2₁/m |
|---|---|---|---|---|---|---|
| Cell volume (Å³) | 902.7(1) | 902.9(1) | 902.66(9) | 902.7(1) | 902.7(1) | 451.23(4) |
| $R_{wp}$ | 0.048 | 0.044 | 0.038 | 0.045 | 0.042 | 0.040 |
| $\chi^2$ | 0.699 | 0.720 | 0.624 | 0.710 | 0.635 | 0.576 |
| $R_{F2}$ | 0.110 | 0.097 | 0.085 | 0.098 | 0.087 | 0.106 |
| No. refined par. | 72 | 117 | 116 | 99 | 103 | 55 |
| Total Mg (apfu) | 9.60 | 9.40 | 9.42 | 9.44 | 9.44 | 10.00* |
| Total Al (apfu) | 9.80 | 10.12 | 10.02 | 10.06 | 10.04 | 10.00* |
| Occ. Mg-X | 0.40 | 0.35 | 0.71,0.00 | 0.72,0.00 | 0.36 | 0.50* |
| Al-X | 0.45 | 0.53 | 0.14,0.87 | 0.49,0.54 | 0.51 | 0.50* |
| Si(2) | 0.83 | 0.83 | 0.25,1.00 | 0.84 | 0.82 | 1.00* |
| Si(2b) | 0.17 | 0.17 | 0.75,0.00 | 0.16 | 0.18 | 0.00* |

*Notes:* The results of the refinement using the sursassite structure model are also listed. The refined occupancies of each site involved in the stacking disorder is shown, together with the total amount of Mg and Al cations obtained from the refinement. See text for details.

$R_{wp}= [\Sigma w(I_o-I_c)^2/\Sigma\ wI_o^2]^{1/2}$　　　$\chi^2=[\Sigma\ w(I_o-I_c)^2/N_{obs}-N_{var}]^{1/2}$　　　$R_{F2}=\Sigma\ |\ F_o^2-F_c^2|\ /\Sigma\ |\ F_o^2|$

* Assumed by stoichiometry.
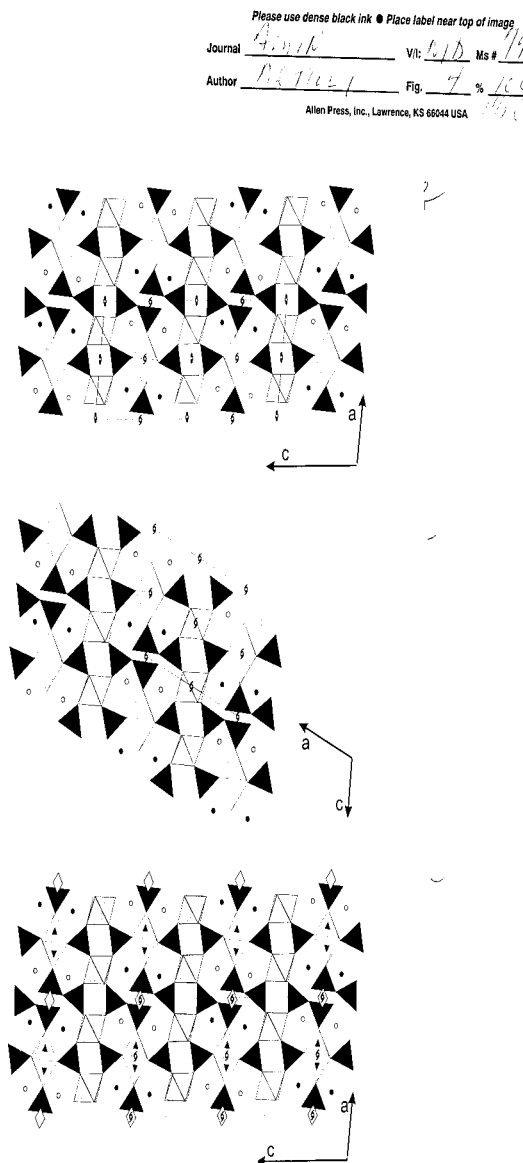


tween successive X-layers. It is therefore not surprising that the most satisfactory structure model in terms of profile agreement indices (Table 1) is in subgroup *P2₁/m*, which is also the only *t* subgroup that has no symmetry elements (twofold axes or *c* glides) relating successive X-layers. It should be noted that the *P2₁/m* structure has the same cell of the parent *A2/m* pumpellyite but the origin is shifted by (0,1/4,1/4).

The model of disorder implies that some of the Si atoms in the X-layer (Si2 atoms located close to the screw axes) are missing, and the absence of a couple of inversion-related tetrahedral Si atoms is linked to the insertion of a Mg atom on the center of symmetry at (0,1/2,1/2), on what is to be considered a nearly perfect octahedrally coordinated site. Since the overall Si content in the cell must be preserved according to the chemical analysis and in order to insure structure stability, the presence of each vacant Si2 site imply the presence of a couple of Si tetrahedra (labeled Si2b sites) substituting for Al in one X-octahedron. Both the Mg atoms at coordinates (0,1/2,0) and the Si2b atoms at (0.36,1/4,0.49) were clearly detected in the difference Fourier maps derived from the refinement.

The disordered model showing the X-octahedra ↔ Si2-tetrahedra substitution is virtually equivalent to a stacking model having some of the X-layers in the sequence shifted by (1/2,0,0) vectors. In MgMgAl-pumpellyite only a small number of layers are shifted: they are assumed to be occupied by Mg atoms,

**FIGURE 4.** The structure of pumpellyite. Top, projection along [010] described in the parent *A2/m* space group (Galli and Alberti 1969). Solid triangles represent Si tetrahedra, and open and shaded octahedra represent X- and Y-octahedral sites respectively. Middle, sursassite-type stacking sequence of layers perpendicular to [001], described in the *P2₁/m* cell of Mn-sursassite (Mellini et al. 1984). Bottom, projection of the structure of MgMgAl-pumpellyite here described in the *P2₁/m* subgroup. The structure disorder in the X-octahedra layers is described by insertion of Mg-octahedral sites (open diamonds) in place of couples of Si tetrahedra, and by insertion of Si tetrahedra (small solid triangles) in place of Mg octahedra. The site disorder model is equivalent to a model having some sursassite-type layers stacked within a pumpellyite-type sequence (see text for details).

**TABLE 2.** Inter-atomic distances (Å) for MgMgAl-pumpellyite ($P2_1/m$ model)

| | | | | | |
|---|---|---|---|---|---|
| Mg1-O1 ×2 | 2.21(2) | Si1)-O1 ×2 | 1.676(9) | X-Al1-O2 ×2 | 2.15(1) |
| Mg1-O3 ×2 | 2.05(2) | Si1)-O4 | 1.66(1) | X-Al1-O9 ×2 | 1.91(1) |
| Mg1-O8 | 2.33(2) | Si1)-O8 | 1.68(1) | X-Al1-O11 ×2 | 1.96(2) |
| Mg1-O11 | 2.07(2) | mean | 1.673 | mean | 2.007 |
| mean | 2.155 | | | | |
| | | Si2-O2 ×2 | 1.708(9) | X-Al2-O13 ×2 | 2.06(1) |
| Mg2-O1 ×2 | 2.10(2) | Si2-O8 | 1.71(1) | X-Al2-O20 ×2 | 1.94(1) |
| Mg2-O2 ×2 | 2.24(2) | Si2-O10 | 1.71(1) | X-Al2-O22 ×2 | 1.91(1) |
| Mg2-O9 | 2.35(2) | mean | 1.709 | mean | 1.970 |
| Mg2-O10 | 2.16(2) | | | | |
| mean | 2.198 | Si2b-O2 ×2 | 1.61(1) | Y-Al1-O3 | 1.95(2) |
| | | Si2b-O9 | 1.68(1) | Y-Al1-O4 | 1.89(2) |
| Mg3-O13 ×2 | 2.22(2) | Si2b-O11 | 1.66(1) | Y-Al1-O5 | 2.01(2) |
| Mg3-O14 ×2 | 2.13(2) | mean | 1.640 | Y-Al1-O12 | 1.96(2) |
| Mg3-O19 | 2.38(2) | | | Y-Al1-O17 | 1.94(2) |
| Mg3-O22 | 2.15(2) | Si3-O3 ×2 | 1.66(1) | Y-Al1-O18 | 1.85(2) |
| mean | 2.205 | Si3-O6 | 1.67(1) | mean | 1.933 |
| | | Si3-O9 | 1.67(1) | | |
| Mg4-O12 ×2 | 2.04(2) | mean | 1.665 | Y-Al2-O1 | 1.95(2) |
| Mg4-O13 ×2 | 2.24(2) | | | Y-Al2-O6 | 1.97(2) |
| Mg4-O20 | 2.34(2) | Si4-O12 ×2 | 1.66(1) | Y-Al2-O7 | 1.91(2) |
| Mg4-O21 | 2.13(2) | Si4-O15 | 1.66(1) | Y-Al2-O14 | 1.94(2) |
| mean | 2.172 | Si4-O19 | 1.66(1) | Y-Al2-O15 | 1.96(2) |
| | | mean | 1.660 | Y-Al2-O16 | 1.96(2) |
| X-Mg1-O2 ×2 | 2.15(1) | | | mean | 1.948 |
| X-Mg1-O8 ×2 | 1.96(1) | Si5-O13 ×2 | 1.648(9) | | |
| X-Mg1-O10 ×2 | 1.99(2) | Si5-O19 | 1.69(1) | | |
| mean | 2.033 | Si5-O21 | 1.68(1) | | |
| | | mean | 1.667 | | |
| X-Mg2-O13 ×2 | 2.24(1) | | | | |
| X-Mg2-O19 ×2 | 1.97(1) | Si5b-O13 ×2 | 1.74(1) | | |
| X-Mg2-O21 ×2 | 2.05(2) | Si5b-O20 | 1.68(1) | | |
| mean | 2.087 | Si5b-O22 | 1.69(1) | | |
| | | mean | 1.713 | | |
| | | Si6-O14 ×2 | 1.661(9) | | |
| | | Si6-O17 | 1.65(1) | | |
| | | Si6-O20 | 1.68(1) | | |
| | | mean | 1.663 | | |

on the basis of the longer cation-oxygen mean distances (2.086 Å) of the cations in 0,1/2,1/2 (hereafter labeled X-Mg position) with respect to the mean distances observed (1.969 Å) for the cations in 1/2,1/2,0 (hereafter labeled X-Al position), and therefore considered to be Al atoms. By this assumption, the total refined occupancies of the Mg and Al sites indicates a slight Mg deficiency and Al excess in the structure with respect to ideal Mg:Al = 1:1 stoichiometry, independently of the assumed space group (Table 1). The discrepancy with respect to the nearly ideal stoichiometry measured by EPMA is probably to be ascribed to the fact that the average structure model showing long-range disorder cannot fully describe the short-range distribution of stacking fault defects. The studied sample also shows a slightly larger cell volume with respect to the one reported by Schreyer et al. (1991). Assuming that the discrepancy is not caused by the different method used to extract the cell parameters (i.e., full profile fitting vs. single-peak indexing and least squares minimization), this could be due to the different density of stacking defects in the two samples.

The site occupancy factors of the X-Mg and X-Al positions in the X-layers of the $P2_1/m$ structure can be refined independently and show marked differences [Table 1: X-Mg(0) = 0.71(5), X-Mg(1/2) = 0.05(5), X-Al(1/2) = 0.14(5), X-Al(0) = 0.87(5)]. The same is observed of course for the related Si2 and Si2b tetrahedral positions. Accordingly, the refined occupancy of the average cation sites in the parent space group and in the other subgroups containing diads or c axes are just mean values of the

real occupancies of the independent sites. Curiously, space group $P2/c$ allows independent positions to be refined for the X-cations, but not for the substituting Si2 and Si2b tetrahedral atoms. Also the subsets of X-Mg and X-Al positions are different than those obtained in space group $P2_1/m$, and it may be readily observed from Table 1 that in space group $P2/c$ the correct occupancies are obtained for the X-Mg positions, whereas mean values are obtained for the X-Al positions.

It should be also noted from the data listed in Table 1 that the site occupancy factors resulting from the refinement in $P2_1/m$ are in agreement with the assumed coupled substitutions (X-Mg ↔ Si2 and X-Al ↔ Si2b), since the sum of occupancies relative to sites that cannot be simultaneously occupied is systematically lower that 1.0 (i.e., distance X-Mg1-Si2 = 1.77(1) Å, combined occupancy 0.71 + 0.25 = 0.96; distance X-Al1-Si2b = 1.86, combined occupancy 0.14 + 0.75 = 0.89; distance X-Mg2-Si5 = 1.93(1), combined occupancy 0.00 + 1.00 = 1.00; distance X-Al2-Si5b = 1.72(1), combined occupancy 0.87 + 0.00 = 0.87). This is not the case for the refinements in the other space groups, where couples of incompatible atoms show combined occupancies significantly larger that 1.0, indicating the presence of model inconsistencies.

In summary, the space group $P2_1/m$ is considered the most satisfactory description of the symmetry of MgMgAl-pumpellyite, taking into account that: (1) it produces significantly better agreement factors for the refinement both in terms of fit ($R_{wp}$, $\chi^2$) and in terms of the structure model ($R_{F2}$); (2) it

accounts well for the small Bragg peaks observed in the powder diffraction pattern and violating the *A* centering of the parent space group; (3) it allows proper modeling of the polytypic structure of MgMgAl-pumpellyite by independent layers containing octahedrally coordinated X-cations; and (4) it yields site occupancy factors for the octahedral and tetrahedral cations which are reasonably consistent with a disordered substitutional model, and they are in good agreement with the expected stoichiometry of the compund.

The final Rietveld refinement of the synchrotron powder pattern was therefore performed in the $P2_1/m$ space group, using the following conditions: the instrumental background was modeled by a polynomial curve (Chebyshev polynomial of the I kind) with 12 refinable coefficients, the Bragg peaks were modeled by a pseudo-Voigt function with one Gaussian and one Lorentzian refinable coefficients, Bragg-peak to background cutoff was assumed at 0.7% of the peak intensity. A single zero shift parameter, one scale factor and the unit-cell parameters of each phase, and the atomic coordinates, site occupancy factors, and atomic isotropic displacement parameters of pumpellyite were simultaneously refined in the last least-squares cycles. Only three isotropic displacement parameters were refined to limit the numbers of refinable parameters: one for the oxygen atoms, one for the tetrahedral silicon atoms, and one for the octahedral cations. Finally, the occupancy factors of the tetrahedral sites were constrained to give full occupancy (Si2 + Si2b = 1.0), whereas those of the octahedral sites were freely refined.

A summary of the Rietveld refinement parameters is listed in Table 3, structural parameters are listed in Table 4, and inter-atomic distances and angles are listed in Table 2. Figure 5 shows the final observed, calculated, and difference powder diffraction patterns.

The resulting crystal structure model for the synthetic high pressure MgMgAl-pumpellyite is broadly consistent with the structure of Ca-rich pumpellyite described in low-grade metamorphic rocks. Although the presence of small Mg cations in place of the Ca atoms in the W sites produces a severe distortion of the structure, the basic building units of pumpellyite are the strips of edge-sharing octahedra along the [010] direction.

**TABLE 3.** Summary of the refinement parameters for MgMgAl-pumpellyite

| | | | |
|---|---|---|---|
| wavelength (Å) | 1.30365(2) | *a* (Å) | 8.5758(4) |
| 2θ range (°) | 7.2–63.4 | *b* (Å) | 5.7295(2) |
| No. observations | 2846 | *c* (Å) | 18.5376(9) |
| No. reflections (pumpellyite) | 587 | β (°) | 97.691(3) |
| No. reflections (coesite) | 160 | *V* (Å³) | 902.66(9) |
| No. variables | 116 | pseudo-Voigt GW | 42.2(1.4) |
| space group | $P2_1/m$ | pseudo-Voigt LX | 3.7(0.3) |

**TABLE 4.** Refined atomic coordinates for MgMgAl-pumpellyite ($P2_1/m$ model)

| Atom | x | y | z | $U_{iso}$ | Occupancy |
|---|---|---|---|---|---|
| Mg1 | 0.294(2) | 3/4 | 0.582(2) | 0.095(2) | 1.0 |
| Mg2 | 0.225(3) | 3/4 | 0.410(1) | 0.095(2) | 1.0 |
| Mg3 | 0.731(2) | 3/4 | 0.909(1) | 0.095(2) | 1.0 |
| Mg4 | 0.818(2) | 3/4 | 0.084(1) | 0.095(2) | 1.0 |
| X-Mg1 | 0 | 1/2 | 1/2 | 0.095(2) | 0.71(5) |
| X-Mg2 | 0 | 1/2 | 0 | 0.095(2) | 0.05(5) |
| X-Al1 | 1/2 | 1/2 | 1/2 | 0.095(2) | 0.14(5) |
| X-Al2 | 1/2 | 1/2 | 0 | 0.095(2) | 0.87(5) |
| Y-Al1 | 0.262(2) | 0.514(4) | 0.752(1) | 0.095(2) | 1.0 |
| Y-Al2 | 0.749(3) | 0.501(4) | 0.746(1) | 0.095(2) | 1.0 |
| Si1 | 0.042(3) | 1/4 | 0.345(1) | 0.104(2) | 1.0 |
| Si2 | 0.122(3) | 1/4 | 0.501(1) | 0.104(2) | 0.25(4) |
| Si2b | 0.360(3) | 1/4 | 0.495(1) | 0.104(2) | 0.75(4) |
| Si3 | 0.438(3) | 1/4 | 0.650(1) | 0.104(2) | 1.0 |
| Si4 | 0.947(3) | 1/4 | 0.157(1) | 0.104(2) | 1.0 |
| Si5 | 0.849(2) | 1/4 | 0.999(1) | 0.104(2) | 1.06(4) |
| Si5b | 0.610(3) | 1/4 | 0.996(1) | 0.104(2) | −0.06(4) |
| Si6 | 0.545(3) | 1/4 | 0.853(1) | 0.104(2) | 1.0 |
| O1 | 0.121(3) | 0.512(3) | 0.332(1) | 0.087(1) | 1.0 |
| O2 | 0.249(1) | 0.477(2) | 0.497(1) | 0.087(1) | 1.0 |
| O3 | 0.357(3) | 0.507(3) | 0.662(1) | 0.087(1) | 1.0 |
| O4 | 0.121(5) | 3/4 | 0.714(3) | 0.087(1) | 1.0 |
| O5 | 0.128(4) | 1/4 | 0.707(2) | 0.087(1) | 1.0 |
| O6 | 0.384(4) | 3/4 | 0.301(3) | 0.087(1) | 1.0 |
| O7 | 0.388(5) | 1/4 | 0.290(3) | 0.087(1) | 1.0 |
| O8 | 0.980(3) | 1/4 | 0.427(1) | 0.087(1) | 1.0 |
| O9 | 0.501(3) | 3/4 | 0.432(1) | 0.087(1) | 1.0 |
| O10 | 0.020(3) | 1/4 | 0.575(1) | 0.087(1) | 1.0 |
| O11 | 0.532(3) | 3/4 | 0.572(1) | 0.087(1) | 1.0 |
| O12 | 0.841(3) | 0.491(4) | 0.160(1) | 0.087(1) | 1.0 |
| O13 | 0.739(1) | 0.486(2) | 0.997(1) | 0.087(1) | 1.0 |
| O14 | 0.664(2) | 0.466(3) | 0.837(1) | 0.087(1) | 1.0 |
| O15 | 0.868(4) | 3/4 | 0.802(3) | 0.087(1) | 1.0 |
| O16 | 0.888(5) | 1/4 | 0.789(3) | 0.087(1) | 1.0 |
| O17 | 0.613(5) | 3/4 | 0.208(3) | 0.087(1) | 1.0 |
| O18 | 0.594(4) | 1/4 | 0.224(2) | 0.087(1) | 1.0 |
| O19 | 0.989(3) | 1/4 | 0.072(1) | 0.087(1) | 1.0 |
| O20 | 0.543(2) | 3/4 | 0.071(1) | 0.087(1) | 1.0 |
| O21 | 0.935(3) | 1/4 | 0.923(1) | 0.087(1) | 1.0 |
| O22 | 0.491(3) | 3/4 | 0.932(1) | 0.087(1) | 1.0 |
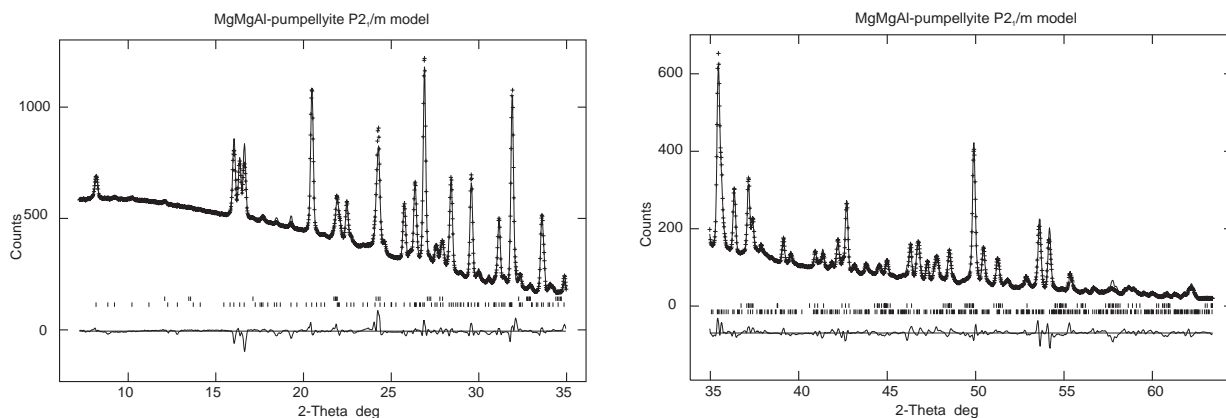


**FIGURE 5.** Observed (solid line), calculated (crosses), and difference powder diffraction patterns for the Rietveld refinement of MgMgAl-pumpellyite. Angular regions are: (**left**) 7.20-35 °2θ, (**right**) 35–63.4 °2θ. The lower and upper vertical bars indicate the position of the Bragg peaks of pumpellyite and coesite, respectively.
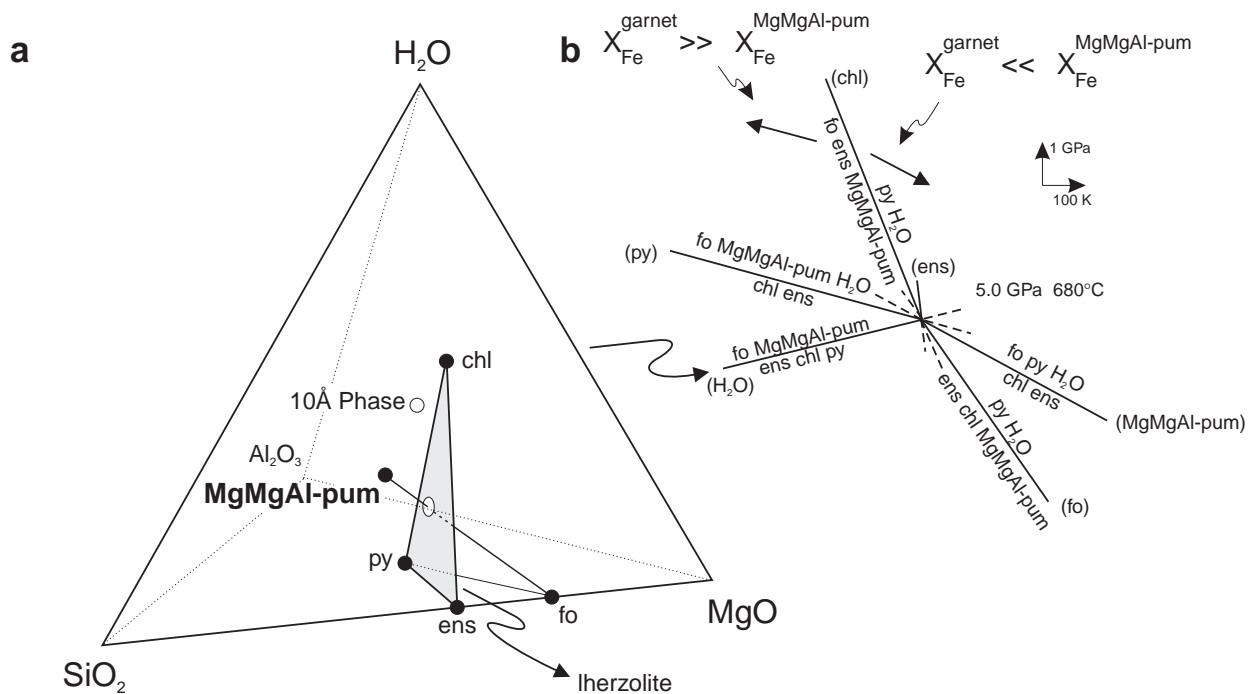
**FIGURE 6.** Phase relations. (**a**) compositional tetrahedron of the MgO-Al₂O₃-SiO₂-H₂O (MASH) model system. The intersection between the shaded plane and the join MgMgAl-pum-fo represents the water-absent reaction detailed in Figure 6b. (**b**) Schreinemakers' bundle around the 10 Å phase invariant point. MgMgAl-pum = MgMgAl-pumpellyite; chl = chlorite; fo = forsterite; ens = enstatite.

The chains composed of Y-octahedra and fully occupied by Al atoms are the backbone of the structure. There are four such chains in the unit cell.

## PHASE RELATIONSHIPS AND PETROGENETIC SIGNIFICANCE

MgMgAl-pumpellyite associated with forsterite and orthoenstatite is stable at 5.2 GPa and 680 °C, is in agreement with the stability field of Fockenberg (1998). Our data provide a preliminary constraint on the topology of this *P-T* region. The absence of chlorite at 5.2 GPa and 680 °C is also consistent, within experimental uncertainties, with the petrogenetic grid in the system MASH reported by Ulmer and Tromsdorff (1998).

Compositional relationships (Fig. 6 left) indicate that there are no terminal reactions involving the phases forsterite, chlorite, enstatite, MgMgAl-pumpellyite, pyrope, and water in the MASH system. The assemblage chlorite + enstatite + pyrope plays a fundamental role in controlling the occurrence of MgMgAl-pumpellyite as it acts as a compositional barrier for most ultramafic compositions, where forsterite is expected. The slopes of the reactions around the 10 Å phase invariant point were estimated at 5.0 GPa and 680 °C (Fig. 6 right) using the thermodynamic properties for forsterite, enstatite, chlorite, and pyrope listed in the Berman database (1988), the H₂O equation of state of Delany and Helgeson (1978), and the volume of MgMgAl-pumpellyite obtained here. Entropy and heat capacity of MgMgAl-pumpellyite were from Grevel (1999) and evaluated from Equation 11 in Berman and Brown (1985), respectively. The [H₂O] reaction was found to be the only one

with a positive d$P$/d$T$ slope. All the other reactions have negative d$P$/d$T$ slopes, including the reaction enstatite + 2 forsterite + MgMgAl-pumpellyite ↔ 5 pyrope + 7 H₂O which is responsible for the disappearance of MgMgAl-pumpellyite at high temperature in ultramafic compositions modeled in the MASH system. Because pyrope + water are expected to be on the high temperature side ($\Delta S > 0$), the large negative $\Delta V$ of reaction (–1.82 J/bar) provides a strong constraint on the negative slope of this pumpellyite breakdown, in contrast with *P-T* diagrams reported in Ulmer and Trommsdorff (1998) and Fockenberg (1995).

Occurrence of an Al-rich phase like MgMgAl-pumpellyite at such pressure-temperature conditions is restricted to bulk compositions containing significant amounts of Fe and Ca, i.e., lherzolites or basalts, but also to materials of sedimentary origin. MgMgAl-pumpellyite was in fact found by Domanik and Holloway (1996) at $P = 7$–8 GPa and $T = 800$–950 °C using natural pelitic sediments as starting materials. The univariant equilibria in simple MASH system become divariant under such conditions, and therefore the evaluation of Fe- and Ca-partitioning between the phases is of primary importance in determining the actual *P-T* field for MgMgAl-pumpellyite bearing assemblages. If we assume, for sake of simplicity, that variations of Fe content in olivine and pyroxene are modest compared to what would be expected in garnet and pumpellyite, then iron partitioning between garnet and pumpellyite solid solutions should be the most relevant parameter to determine experimentally. In principle, if $x_{Fe}$ (garnet) >> $x_{Fe}$ (MgMgAl-pumpellyite) then the breakdown reaction forsterite + enstatite + MgMgAl-pumpellyite ↔ garnet + H₂O moves toward lower

temperatures along the pyrope-absent reaction, chl + ens $\leftrightarrow$ fo + MgMgAl-pumpellyite + $H_2O$. By contrast, assuming $x_{Fe}$ (garnet) $\ll x_{Fe}$ (MgMgAl-pumpellyite) then the same reaction will move toward higher temperatures along the MgMgAl-pumpellyite absent reaction, chl + ens $\leftrightarrow$ fo + pyrope + $H_2O$ (Fig. 6 right). Similar line of reasoning can be applied to Ca-distribution, once solid solution between Ca-bearing pumpellyite and MgMgAl-pumpellyite is assumed.

To clarify the role of MgMgAl-pumpellyite in ultramafic systems at subduction zone conditions, the pressure and temperature stability field of MgMgAl-pumpellyite + forsterite in the model system (Fe,Ca-)MASH has to be compared with *P-T* paths for subducted oceanic lithosphere (Kincaid and Sacks 1997). The higher the Fe and Ca are partitioned into MgMgAl-pumpellyite, the greater its relevance becomes to subduction processes; whereas, Fe,Ca-free MgMgAl-pumpellyite is expected to be present only in substantially colder subducting slabs.

## REFERENCES CITED

Akasaka, M., Kimura, Y., Omori, Y., Sakakibara, M., Shinno, I., and Togari, K. (1997) [57]Fe Mössbauer study of pumpellyite-okhotskite-julgoldite series of minerals. Mineralogy and Petrology, 61, 181–198.

Allmann, R. and Donnay, G. (1973) The crystal structure of julgoldite. Mineralogical Magazine, 39, 271–281.

Angel, R.J., Chopelas, A., and Ross, N.L. (1992) Stability of high-density clinoenstatite at upper-mantle pressures. Nature, 358, 322–324.

Artioli, G. and Geiger, C.A. (1994) The crystal chemistry of pumpellyite: an X-ray Rietveld refinement and [57]Fe Mössbauer study. Physics and Chemistry of Minerals, 20, 443–453.

Artioli, G., Pavese, A., Bellotto, M., Collins, S.P., and Lucchetti, G. (1996) Mn crystal chemistry in pumpellyite: a resonant scattering powder diffraction Rietveld study using synchrotron radiation. American Mineralogist, 81, 603–610.

Berman, R.G. (1988) Internally-consistent thermodynamic data for minerals in the system $Na_2O$-$K_2O$-CaO-MgO-FeO-$Fe_2O_3$-$Al_2O_3$-$SiO_2$-$TiO_2$-$H_2O$-$CO_2$. Journal of Petrology, 29, 445–522.

Berman, R.G. and Brown, T.H. (1985) Heat capacity of minerals in the system $Na_2O$-$K_2O$-CaO-MgO-FeO-$Fe_2O_3$-$Al_2O_3$-$SiO_2$-$TiO_2$-$H_2O$-$CO_2$: representation, estimation, and high temperature extrapolation. Contribution to Mineralogy and Petrology, 89, 168-183.

Coombs, D.S., Kawachi, Y., and Ford, P.B. (1996) Porphyroblastic mangaxinite metapelagites with incipient garnet in prehnite-pumpellyite facies, ner Meyers Pass, Torlesse Terrane, New Zealand. Journal of Metamorphic Geology, 14, 125–142.

Delany, J.M. and Helgeson, H.C. (1978) Calculation of the thermodynamic consequences of dehydration in subducting oceanic crust to 100 kb and > 800 °C. American Journal of Science, 278, 638–686.

Domanik, K.J. and Holloway, J.R. (1996) The stability and composition of phengitic muscovite and associated phases from 5.5 to 11 GPa: implications for deeply subducted sediments. Geochimica et Cosmochimica Acta, 60, 4133–4150.

Ferraris, G., Mellini, M., and Merlino, S. (1986) Polysomatism and the classification of minerals. Rendiconti della Società Italiana di Mineralogia e Petrologia, 41, 181–192.

Fockenberg, T. (1995) New experimental results up to 100 kbar in the system MgO-$Al_2O_3$-$SiO_2$-$H_2O$ (MASH): Preliminary stability fields of chlorite, chloritoid, staurolite, MgMgAl-pumpellyite, and pyrope. Bochumer Geologischeand Geotechnische Arbeiten, 44, 39–44.

———(1998) An experimental study of the pressure-temperature stability of MgMgAl-

pumpellyite in the system MgO-$Al_2O_3$-$SiO_2$-$H_2O$. American Mineralogist, 83, 220–227.

Galli, E. and Alberti, A. (1969) On the crystal structure of pumpellyite. Acta Crystallographica, B25, 2276–2281.

Gottardi, G. (1965) Die kristallstruktur von pumpellyit. Tschermaks Mineralogische und Petrographische Mitteilungen, 10, 115–119.

Grevel, K-D. (1999) High temperature oxide melt solution calorimetry of MgMgAl-pumpellyite. Terra Abstracts, 11, 705.

Hamilton, D.L. and Henderson, C.M.B. (1968) The preparation of silicate composition by gelling method. Mineralogical Magazine, 36, 832–838.

Hammersley, A.P., Svensson, S.O., Hanfland, M., Fitch, A.N., and Häusermann, D. (1996) Two-dimensional detector software: from real detector to idealised image or two-theta scan. High Pressure Research, 14, 235–248.

Ivanov, O.K., Arkhangel'skaya, L.O., Miroshinikova, L.O., and Shilova, T.A. (1981) Shuiskite, the chromium analogue of pumpellyite, from the Bisersk deposit. Zapiski Vsesoyuznogo Mineralogicheskogo Obshchestva, 110, 508–512.

Kincaid, C. and Sacks, I.S. (1997) Thermal and dynamical evolution of the upper mantle in subduction zones. Journal of Geophysical Research, 102, 12295–12315.

Larson, A.C. and Von Dreele, R.B. (1998) GSAS General Structure Analysis System. Report LAUR 86-748. Los Alamos National Laboratory, Los Alamos, New Mexico.

Mellini, M., Merlino, S., and Pasero, M. (1984) X-ray and HRTEM study of sursassite: crystal structure, stacking disorder, and sursassite-pumpellyite intergrowth. Physics and Chemistry of Minerals, 10, 99–105.

Moore, P.B. (1971) Julgoldite, the $Fe^{+2}$–$Fe^{+3}$ dominant pumpellyite. Lithos, 4, 93–99.

Pan, Y. and Fleet, M.E. (1992) Vanadium-rich minerals of the pumpellyite group from the Hemlo gold deposit, Ontario. Canadian Mineralogist, 30, 153–162.

Pascarelli, S., Boscherini, F., D'Acapito, F., Hardy, J., Meneghini, C., and Mobilio, S. (1996) X-ray optics of a dynamical sagittal focus monochromator on the Gilda beamline at the ESRF. Journal of Synchrotron Radiation, 3, 147–152.

Pasero, M. and Reineke, T. (1991) Crystal chemistry, HRTEM analysis and polytypic behaviour of ardennite. European Journal of Mineralogy, 3, 819–830.

Passaglia, E. and Gottardi, G. (1973) Crystal chemistry and nomenclature of pumpellyites and julgoldites. Canadian Mineralogist, 12, 219–223.

Poli, S. and Schmidt, M. (1998) The high-pressure stability of zoisite and phase relationships of zoisite-bearing assemblages. Contributions to Mineralogy and Petrology, 130, 162–175.

Schiffmann, P. and Liou, J.G. (1980) Synthesis and stability relations of Mg-Al pumpellyite, $Ca_4Al_5MgSi_6O_{21}(OH)_7$. Journal of Petrology, 21, 441–474.

Schreyer, W., Maresch, W.V., Medenbach, O., and Baller, T. (1986). Calcium-free pumpellyite, a new synthetic hydrous Mg-Al-silicate formed at high pressures. Nature, 321, 510–511.

Schreyer, W., Maresch, W.V., and Baller, T. (1987). MgMgAl-pumpellyite: A new hydrous high-pressure, synthetic silicate resulting from Mg-for-Ca substitution. Terra Cognita, 7, 385.

Schreyer, W., Maresch, W.V., and Baller, T. (1991). A new hydrous, high-pressure phase with a pumpellyite structure in the system MgO-$Al_2O_3$-$SiO_2$-$H_2O$. In L.L. Perchuk, Ed. Progress in Metamorphic and Magmatic Petrology, p. 47–64. Cambridge University Press.

Susaki, J., Akaogi, S., and Shimura, O. (1985) Garnet-perovskite transformation in $CaGeO_3$: in-situ X-ray measurements using synchrotron radiation. Geophysical Reasearch Letters, 12, 729–732.

Togari, K. and Akasaka, M. (1987) Okhotskite, a new mineral, an $Mn^{3+}$-dominant member of the pumpellyite group, from the Kokuriki mine, Hokkaido, Japan. Mineralogical Magazine, 51, 611–614.

Ulmer, P. and Trommsdorff, V. (1998) Phase relations of hydrous mantle subducting to 300 km. In: Y-W. Fei, C. Bertka, and B.O. Mysen, Eds. Mantle Petrology: Field observations and high-pressure experimentation, in press. Geochemical Society.

Yamamoto, K. and Akimoto, S. (1977) The system MgO-$SiO_2$-$H_2O$ at high pressures and temperatures- stability field for hydroxyl-chondrodite, hydroxyl-clinohumite and 10Å-phase. American Journal of Science, 277, 288–312.

Yoshiasa, A. and Matsumoto, T. (1985) Crystal structure refinement and crystal chemistry of pumpellyite. American Mineralogist, 70, 1011–1019.

Zhang, J., Li, B., Utsumi, W., and Liebermann, R.C. (1996) In situ X-ray observations on the coesite-stishovite transition: Reversed phase boundary and kinetics. Physics and Chemistry of Minerals, 23, 1–10.